Supporting Information for:

A Mechanistic Analysis of Phase Evolution and Hydrogen Storage Behavior in Nanocrystalline $Mg(BH_4)_2$ within Reduced Graphene Oxide

Sohee Jeong[1], Tae Wook Heo[2], Julia Oktawiec[3,7], Rongpei Shi[2], ShinYoung Kang[2], James L. White[4], Andreas Schneemann[4], Edmond W. Zaia[1], Liwen F. Wan[2], Keith G. Ray[2], Yi-Sheng Liu[5], Vitalie Stavila[4], Jinghua Guo[5,6], Jeffrey R. Long[3,7,8], Brandon C. Wood[2], Jeffrey J. Urban[1*]

[1] The Molecular Foundry, Materials Sciences Division, Lawrence Berkeley National Laboratory, Berkeley, California 94720, USA

[2] Materials Science Division, Lawrence Livermore National Laboratory, Livermore, California 94550, USA

[3] Department of Chemistry, University of California, Berkeley, California 94720, USA

[4] Chemistry, Combustion, and Materials Science Center, Sandia National Laboratories, Livermore, California 94550, USA

[5] Advanced Light Source, Lawrence Berkeley National Laboratory, Berkeley, California 94720, USA

[6] Department of Chemistry and Biochemistry, University of California, Santa Cruz, California 95064, USA

[7] Materials Sciences Division, Lawrence Berkeley National Laboratory, Berkeley, California, 94720, USA

[8] Department of Chemical and Biomolecular Engineering, University of California, Berkeley, California, 94720, USA

KEYWORDS

magnesium borohydride, hydrogen storage, phase evolution, thermodynamics, kinetic, reduced graphene oxide

Table S1. Unit cell parameters determined *via* Rietveld refinement using synchrotron powder X-ray diffraction data of Sample **1**, $Mg(BH_4)_2{\cdot}S(CH_3)_2)_{0.42}$, and the phases $Mg(BH_4)_2{\cdot}S(CH_3)_2)_{0.41}$, α-$Mg(BH_4)_2$, and γ-$Mg(BH_4)_2$ in sample **2**. The goodness-of-fit parameters, as defined by TOPAS, are listed for each respective refinement.[2]

	$Mg(BH_4)_2{\cdot}S(CH_3)_2)_n$ in sample 1	$Mg(BH_4)_2{\cdot}S(CH_3)_2)_n$ in sample 2	α-$Mg(BH_4)_2$ in sample 2	γ-$Mg(BH_4)_2$ in sample 2
Space group	Cc	Cc	$P6_122$	$Ia\bar{3}d$
***a* / Å**	7.6380(9)	7.6357(7)	10.3545(15)	15.792(3)
***b* / Å**	13.8535(17)	13.8496(13)	10.3545(15)	15.792(3)
***c* / Å**	12.9343(18)	12.9324(13)	37.092(7)	15.792(3)
***β* (°)**	111.105(3)	111.095(2)	90	90
***V* / Å^3**	1276.8(3)	1276.0(2)	3444.1(12)	3938(2)
R_{exp}	5.22	5.16	5.16	5.16
R_{wp}	2.70	2.43	2.43	2.43
R_p	2.03	1.70	1.70	1.70
R_{Bragg}	1.29	1.59	3.86	1.05
GoF	0.52	0.47	0.47	0.47
Wavelength (Å)	0.499316	0.499316	0.499316	0.499316
Temperature	room temperature	room temperature	room temperature	room temperature
Wt. %	100%	88.4(4)%	9.7(3)%	1.95(8)%
$S(CH_3)_2$ occ.	83.9(9)%	82.2(4)%	–	–

Analysis was first attempted on both sample **1** (dried under vacuum for 3 min) and **2** (dried under Ar overnight), using the previously reported structure of $Mg(BH_4)_2{\cdot}S(CH_3)_2)_n$.[1] Precise unit cell parameters of sample **1** were obtained by structureless Pawley refinement, as implemented in TOPAS-Academic 4.1, and were consistent with those observed previously.[2] However, the previously determined structural model was a clear mismatch to the material (Figure S1). As a result, it was necessary to determine the structure by *ab initio* methods, specifically, the simulated annealing technique as implemented in TOPAS-Academic. Towards this end, each of the BH_4^- units and the $S(CH_3)_2$ in the material was modelled as idealized, rigid bodies using bond angles and distances for these moieties established in the literature as references.[3] In addition, in order to obtain globally minimized results that were chemically reasonable, "anti-bump" penalties were applied to B···C, H···H, Mg···H, and S···H contacts to prevent these contacts from becoming too small.

Once a reasonable structural model was found for sample **1**, a complete Rietveld refinement was performed while maintaining the rigid bodies for the BH_4^- units and the $S(CH_3)_2$ moieties. The thermal parameters (with the exception of those for all H atoms), the positions and orientations of the rigid bodies were freely refined. In addition, a single occupancy factor for the $S(CH_3)_2$ unit was refined, as were the isotropic thermal parameters of all non-H atoms, the thermal parameters of the Mg^{2+} ions, and the Mg^{2+} atomic positions. During the last Rietveld refinement, a final R_{wp} of 2.70% was obtained (Table S1), and the fit showed excellent agreement to the experimental diffraction pattern (Figure 1c).

Upon performing the structureless Pawley refinement using data obtained for sample **2**, it was clear that the sample could not solely be described by similar unit cell parameters, but either contained an entirely new phase or a mixture of multiple phases (Figure S2). Multiple attempts to index the pattern using the Single Value Decomposition approach [4] and then modeling all of the observed peaks with one phase through a structureless Pawley refinement failed. In addition, the diffraction pattern of sample **2** seemed to be consistent with the presence of both α-$Mg(BH_4)_2$ and γ-$Mg(BH_4)_2$, in addition to the phase of $Mg(BH_4)_2{\cdot}(S(CH_3)_2)_{0.42}$ found in sample **1**, leading us to conclude that a three-component mixture containing these phases was an adequate description of the sample and an assignment consistent with other experimental evidence.[5,6] It should be noted that refinements with just one of those components, or only two, did not yield adequate goodness-of-fit parameters and quite clearly did not account for all of the observed reflections.

The structural model for $Mg(BH_4)_2{\cdot}S(CH_3)_2)_{0.42}$ determined for sample **1** was incorporated into the multicomponent Rietveld refinement of sample **2**, along with the previously reported structural models of α-$Mg(BH_4)_2$ and γ-$Mg(BH_4)_2$.[5,6] The atomic positions of the two minor phases were not refined. However, the scale factors of each phase, the occupancy of the $S(CH_3)_2$ unit in $Mg(BH_4)_2{\cdot}(S(CH_3)_2)_n$, the unit cell parameters of every phase, the peak shape parameters, and background and instrument parameters were refined freely. During the last Rietveld refinement, a final R_{wp} of 2.43% was obtained (Table S1), and the fit showed excellent agreement to the experimental diffraction pattern (Figure S2). It should be noted that both sample **1** and sample **2** showed a low GoF parameter (~0.5), which we believe is due to the high level of background present in these samples. However, the major crystalline components are clearly those that we have confirmed by Rietveld refinement.

The volume-weighted apparent crystal size for the α phase of $Mg(BH_4)_2$ in sample **2** was determined by utilizing the integral breadth-based, volume-weighted column heights, as calculated using the peak profile parameters (specifically, CS_G and CS_L as defined in TOPAS). This calculation led to a value of approximately 31 nm for the α phase.

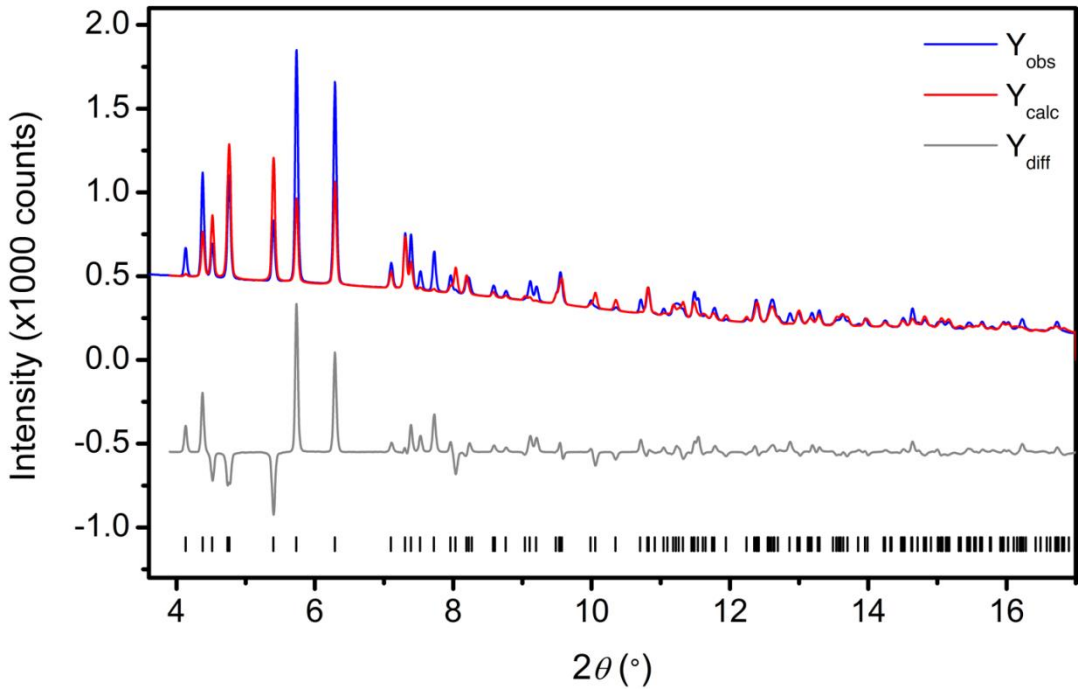

Figure S1. Rietveld refinement of sample **1** at room temperature from 3.8° to 17°, using a previously determined structural model (λ = 0.499316 Å).[1] Blue and red lines represent the observed and calculated diffraction patterns, respectively. The gray line represents the difference between observed and calculated patterns, and the black tick marks indicate calculated Bragg peak positions. As can be seen in the difference curve, there is a significant mismatch in intensities, which we attribute to this sample likely having a different structure.

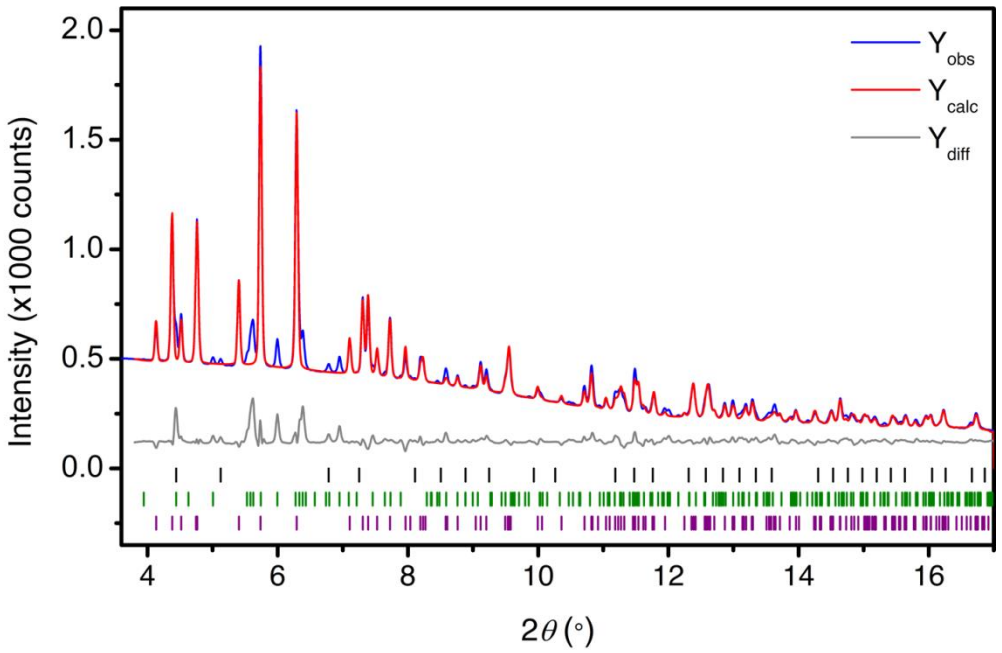

Figure S2. Rietveld refinement with powder X-ray diffraction data of sample **2** at room temperature from 3.8° to 17°, with only the structural model of $Mg(BH_4)_2 \bullet (S(CH_3)_2)_{0.41}$ (λ = 0.499316 Å). Blue and red lines represent the observed and calculated diffraction patterns, respectively. The gray line represents the difference between observed and calculated patterns, and the black, green, and purple tick marks indicate calculated Bragg peak positions for the α-$Mg(BH_4)_2$, γ-$Mg(BH_4)_2$, and $Mg(BH_4)_2 \cdot (S(CH_3)_2)_{0.41}$ phases, respectively. It is clear that the contribution of $Mg(BH_4)_2 \cdot (S(CH_3)_2)_{0.41}$ does not account for all of the diffraction observed. Additional peaks not found in the contribution of $Mg(BH_4)_2 \cdot (S(CH_3)_2)_{0.41}$ at 5°, 5.6°, 6°, 6.8°, 6.9°, and so forth can be clearly distinguished, which are accounted for in the α-$Mg(BH_4)_2$ and γ-$Mg(BH_4)_2$ phases.

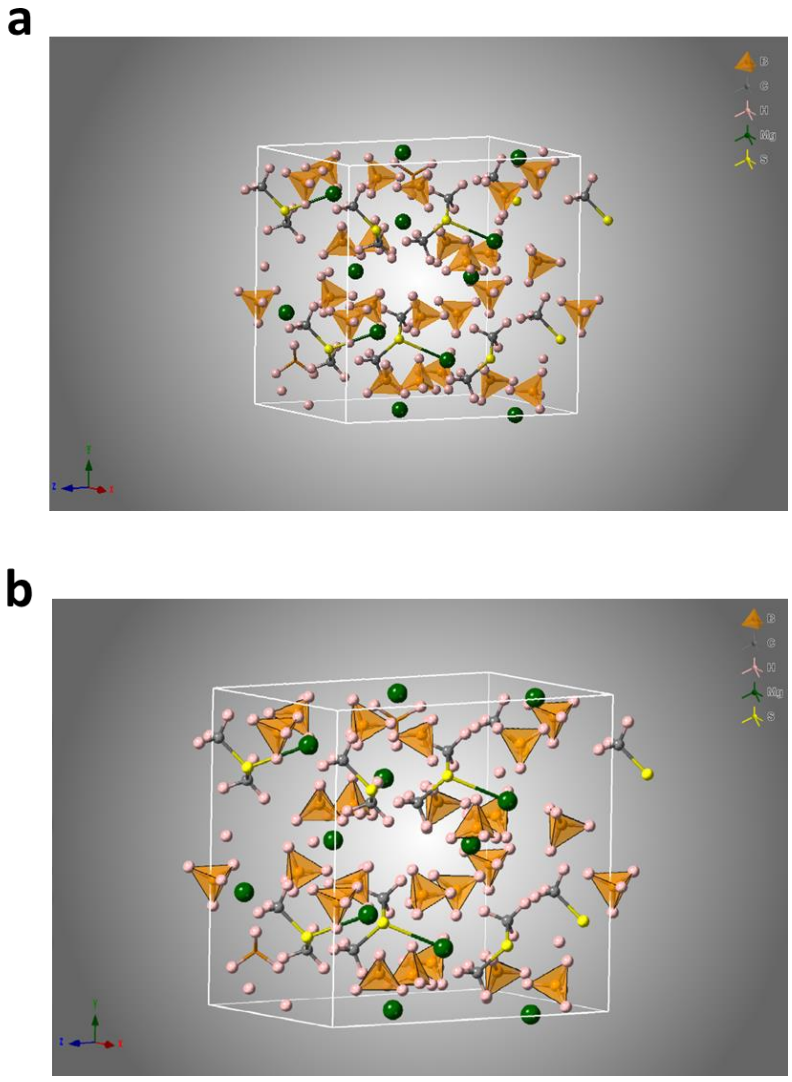

Figure S3. Structural model of (a) $Mg(BH_4)_2{\cdot}S(CH_3)_2)_{0.42}$ in sample **1** and (b) $Mg(BH_4)_2{\cdot}S(CH_3)_2)_{0.41}$ in sample **2**. Green, yellow, gray, and pink spheres represent Mg, S, C, and H atoms, respectively. Boron atoms are at the center of each of the orange tetrahedra.

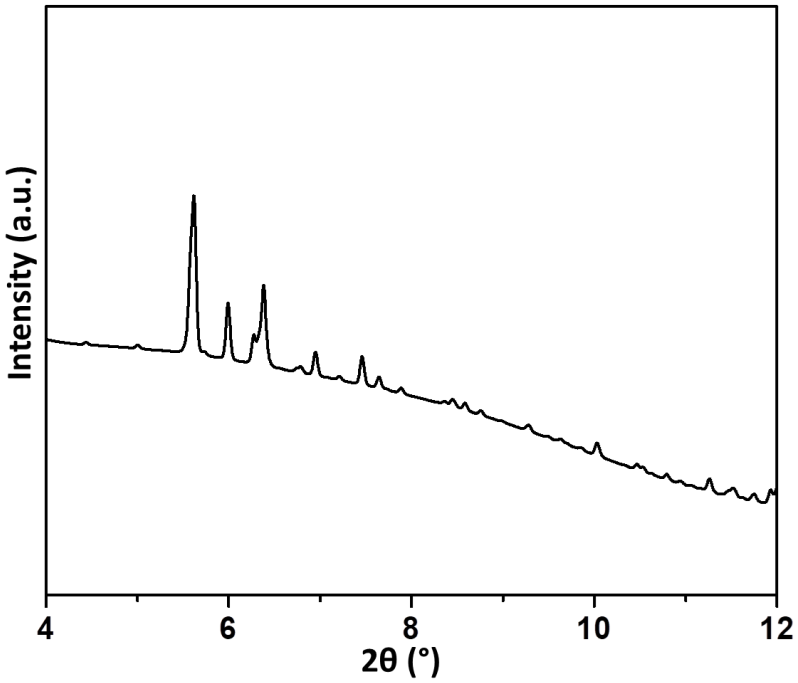

Figure S4. Deconvoluted powder X-ray diffraction (PXRD) pattern of the α phase from the PXRD pattern of sample **2** (λ = 0.499316 Å, see also Figure 1d in the main text).

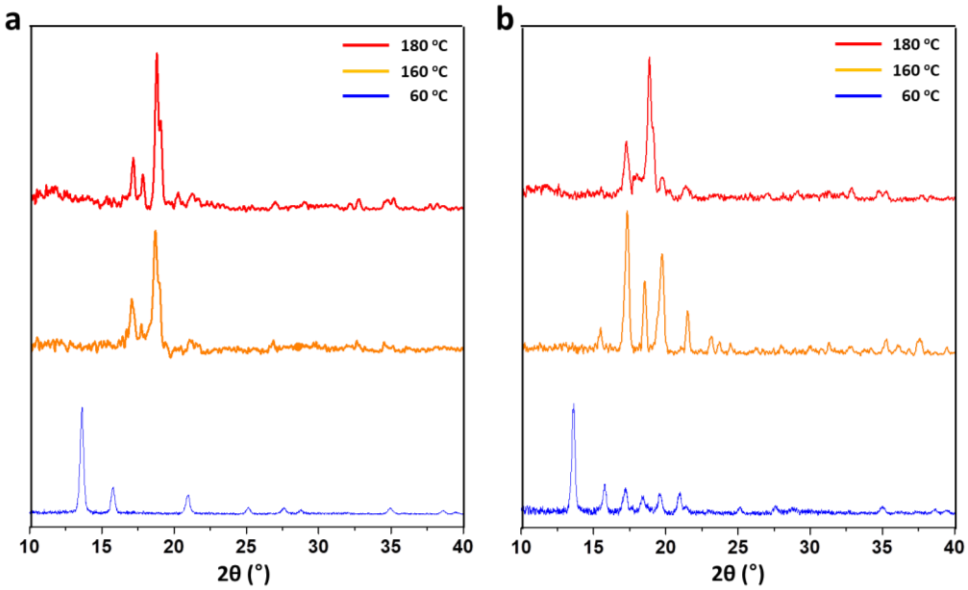

Figure S5. a,b) Phase expression in magnesium borohydride without rGO achieved at 60, 160, and 180 °C by using the solid which was dried under vacuum (a) or under Ar (b) (λ = 1.54056 Å).

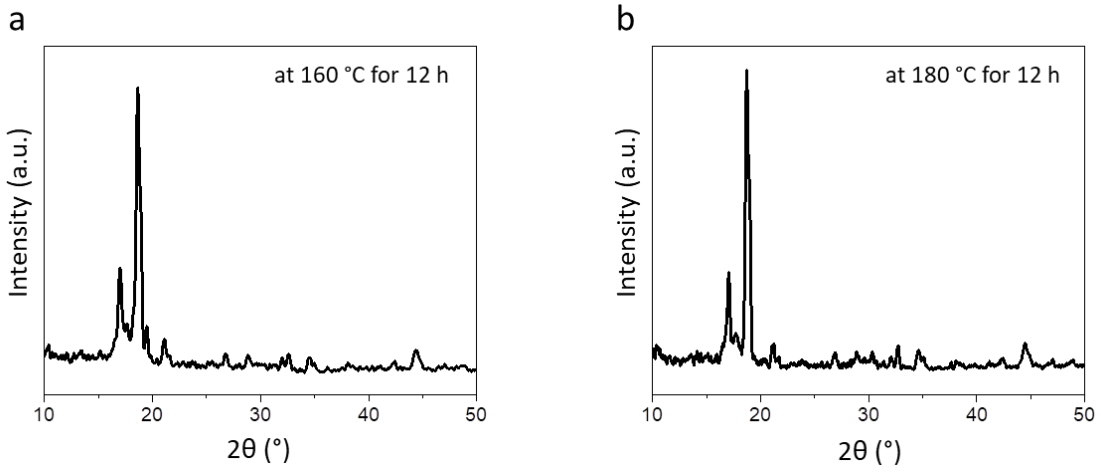

Figure S6. Powder X-ray diffraction patterns of MBHg after annealing sample 1 at 160 °C (a) and 180 °C (b) for 12 h (λ = 1.54056 Å).

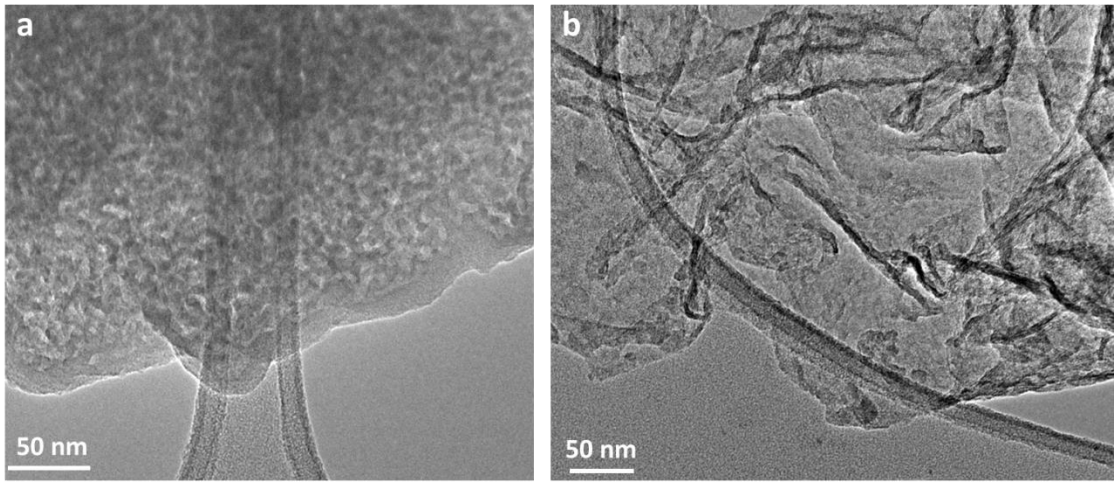

Figure S7. TEM images of a) aggregated and b) dispersed particles obtained after annealing sample **2** at 60 °C.

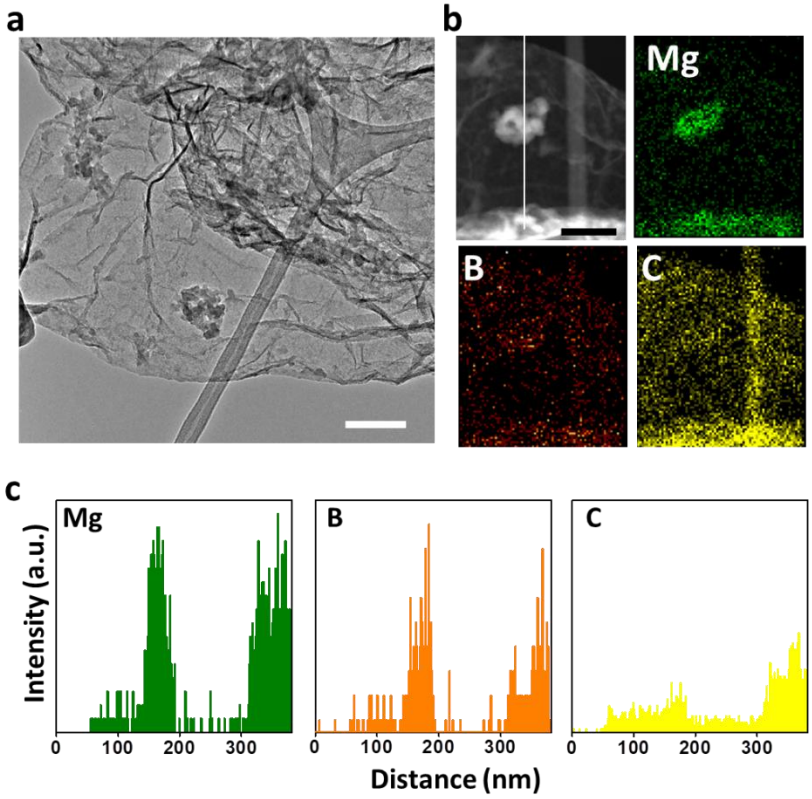

Figure S8. a) TEM image of β-MBHg. b) STEM image and the corresponding energy dispersive X-ray spectroscopy (EDS) mapping of β-MBHg for Mg, B, and C, respectively. c) EDS line mapping corresponding to the white line in part (b). Scale bar:100 nm

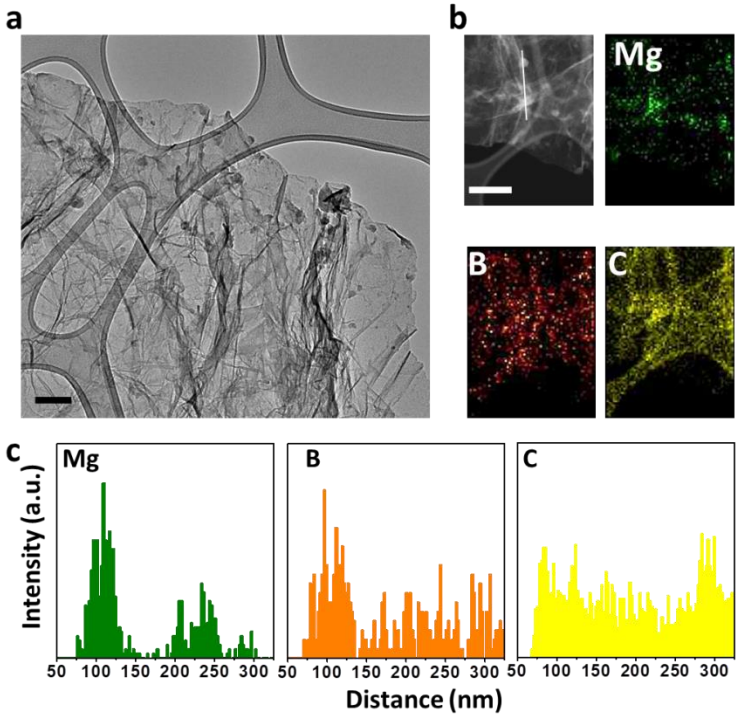

Figure S9. a) TEM image of α-MBHg. b) STEM image and the corresponding EDS mapping of α-MBHg for Mg, B, and C, respectively. c) EDS line mapping corresponding to the white line in part (b). Scale bar: 100 nm

The average crystallite size of $Mg(BH_4)_2$ was determined using the Scherrer Equation:

$$D = \frac{0.9\,\lambda}{\beta \cos\theta}$$

where D is the size of the crystal, λ is the X-ray wavelength (Cu Kα: 0.154 nm or Co Kα: 0.179 nm), β is the full width at half maximum (FWHM) of the diffraction peak, and θ is the Bragg angle. Three samples were examined, as described in the table below.

Table S2. Average crystallite size of γ-$Mg(BH_4)_2$, as determined by PXRD.

γ-phase (X-ray source)	**2 theta (°)**	**FWHM**	**Size (nm)**	**Mean size (nm)**
1 (Cu)	13.643	0.004721	29.56974	27.04847 (σ=2.083543)
	15.7927	0.004688	29.84884	
	20.9855	0.004814	29.28297	
2 (Cu)	13.68438	0.29839	26.81797	
	15.82192	0.31096	25.79612	
	20.99503	0.29494	27.39699	
3 (Co)	15.78896	0.37541	24.83523	
	18.29136	0.37288	25.08567	
	24.35472	0.38091	24.80273	

Table S3. Average crystallite size of β-$Mg(BH_4)_2$, as determined by PXRD.

β-phase (X-ray source)	**2 theta (°)**	**FWHM**	**Size (nm)**	**Mean size (nm)**
1 (Cu)	17.08247	0.27718	28.98597	28.84221 (σ=7.719773)
	17.78429	0.34113	17.37933	
	18.73147	0.23948	23.57423	
2 (Cu)	17.08831	0.31159	29.97104	
	17.76105	0.25472	36.69551	
	18.69372	0.21671	43.1881	
3 (Cu)	17.10114	0.32923	24.40399	
	17.79049	0.49096	16.38004	
	18.75217	0.35388	22.75575	

Table S4. Average crystallite size of α-$Mg(BH_4)_2$, as determined by PXRD.

α-phase (X-ray source)	**2 theta (°)**	**FWHM**	**Size (nm)**	**Mean size (nm)**
1 (Cu)	15.32892	0.21246	37.73343	28.35793 (σ=6.581265)
	17.19566	0.31081	25.8535	
	18.41918	0.27594	29.16931	
	19.5781	0.35777	22.53574	
	21.40216	0.20156	40.1163	
2 (Co)	17.8407	0.2818	33.17281	
	20.00501	0.3978	23.57358	
	21.41855	0.33554	28.01077	
	22.79405	0.48427	19.4536	
	24.91934	0.27255	34.70108	
3 (Co)	17.83684	0.4155	22.49831	
	20.00757	0.39939	30.13494	
	21.42207	0.31189	23.47982	
	22.7924	0.47046	20.02459	
	24.92001	0.27091	34.9112	

Mass at 2-3 amu represents H_2 in the following closed ion source Mass spectra (Figure S8-S10). Masses from 11-13 and 23-28 represent BH_3 and B_2H_6 fragments. Masses at 15 and 29 amu represent hydrocarbon fragments (CH_3, C_2H_5) released from rGO at higher temperatures). Mass at 28 and 31 represent CO and CH_2O released from rGO at elevated temperatures. Signal around m/z = 44 amu represents CO_2 Mass at 18 represents H_2O (i.e. prominent at low temperatures, ambient H_2O adsorbed on the tubings of the reactor, parts of the set up that get exposed to ambient air during sample change). Compared to the H_2 release only very minor amounts of impurities are released during the desorption process.

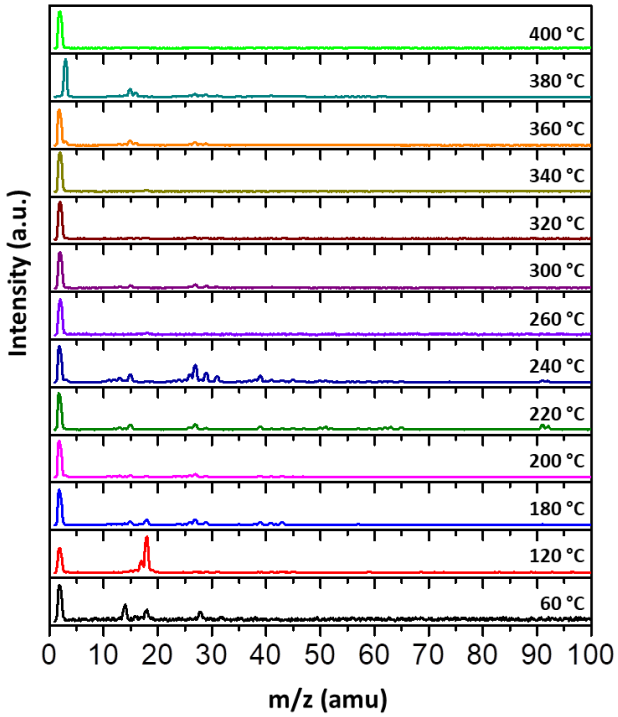

Figure S10. Mass spectra of γ-MBHg recorded at different temperatures in a m/z range from 0-100 amu.

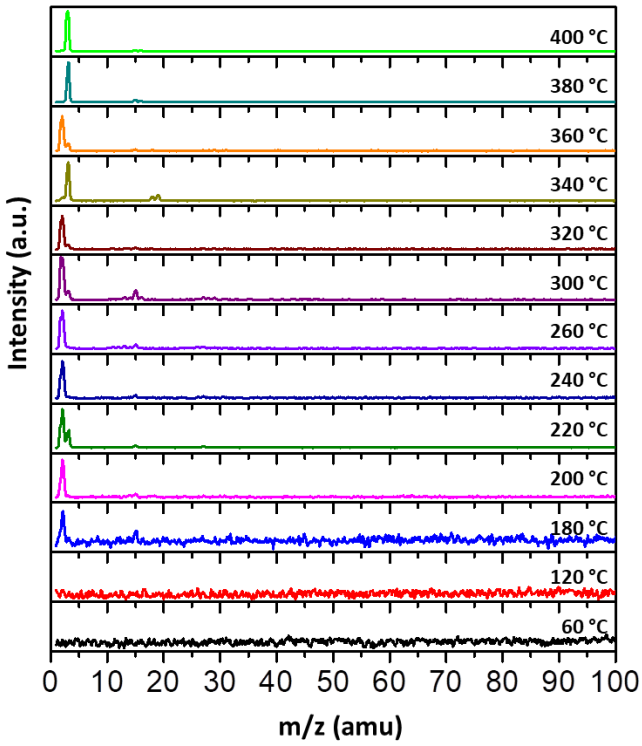

Figure S11. Mass spectra of β-MBHg recorded at different temperatures in a m/z range from 0-100 amu.

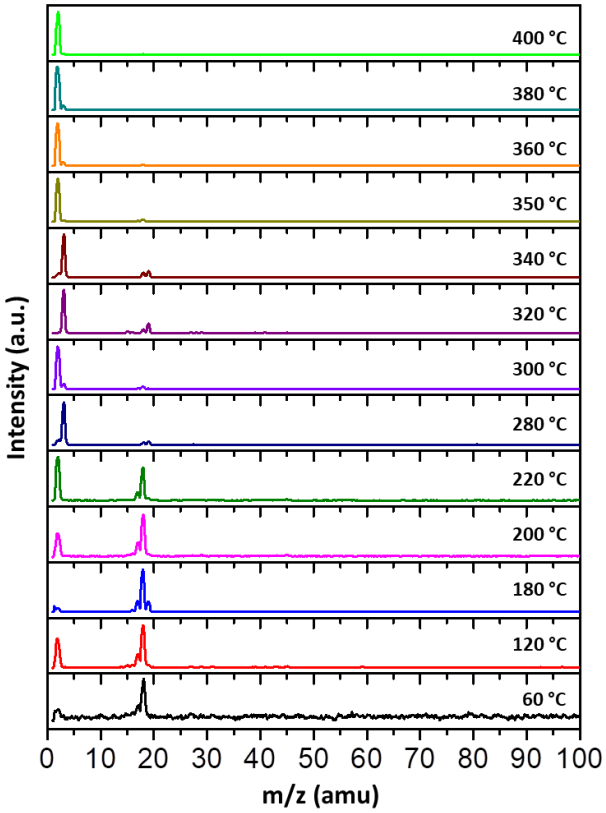

Figure S12. Mass spectra of α-MBHg recorded at different temperatures in a m/z range from 0-100 amu.

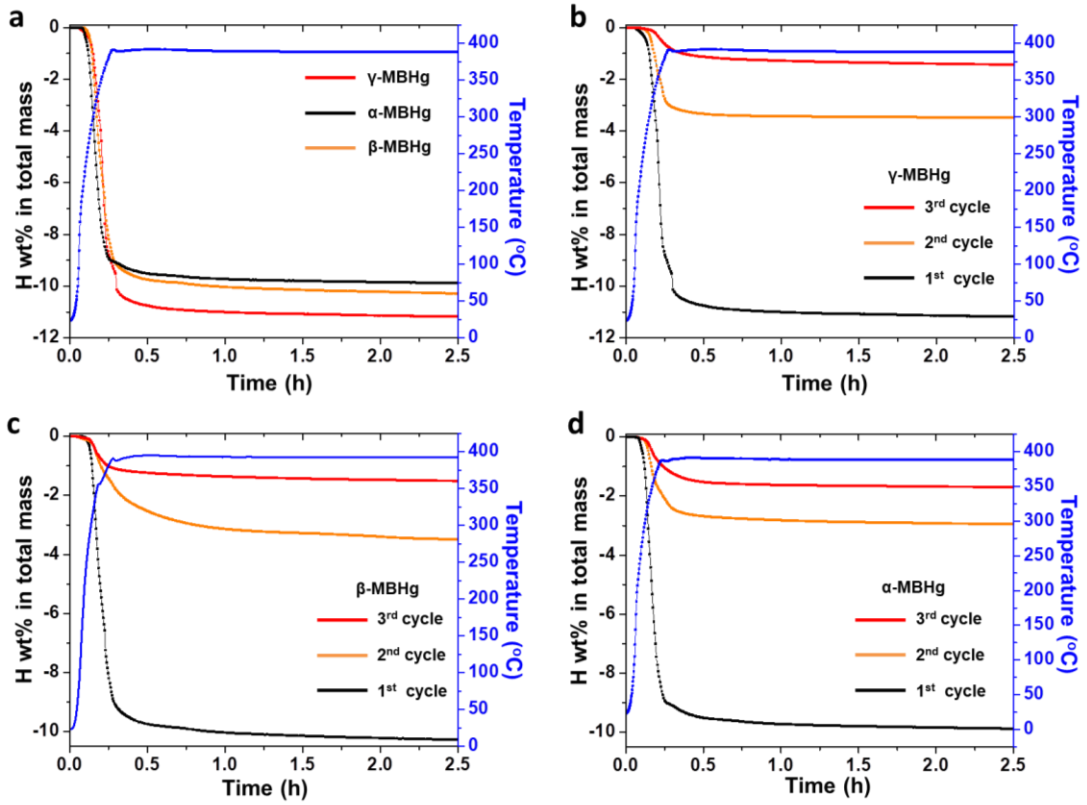

Figure S13. Hydrogen desorption characterization of MBHg. a) Hydrogen desorption (at 390 °C and 0 bar) for the prepared γ, α, and β phases. Hydrogen desorption cycling of (b) γ, (c) β, and (d) α phases of MBHg were performed at 390 °C and 0 bar. The second and third cycles were performed after rehydrogenations at 400 °C and 700 bar for 48 h.

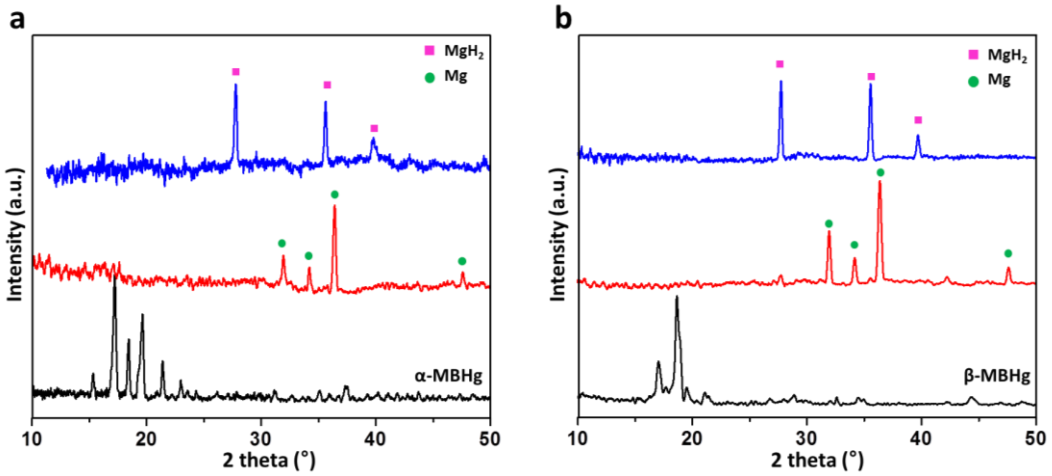

Figure S14. Powder X-ray diffraction patterns of as-synthesized (black), dehydrogenated (red), rehydrogenated (blue) (a) α- and (b) β-MBHg with markers for MgH_2 (pink squares) and Mg (green circles) peaks.

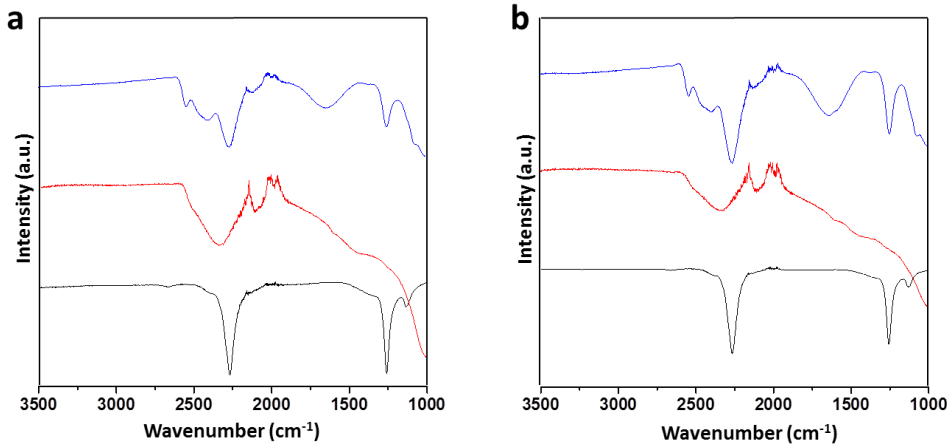

Figure S15. FT-IR spectra of the de/rehydrogenation products in (a) α- and (b) β-MBHg: as-synthesized (black), dehydrogenated (red), and rehydrogenated (blue) MBHg.

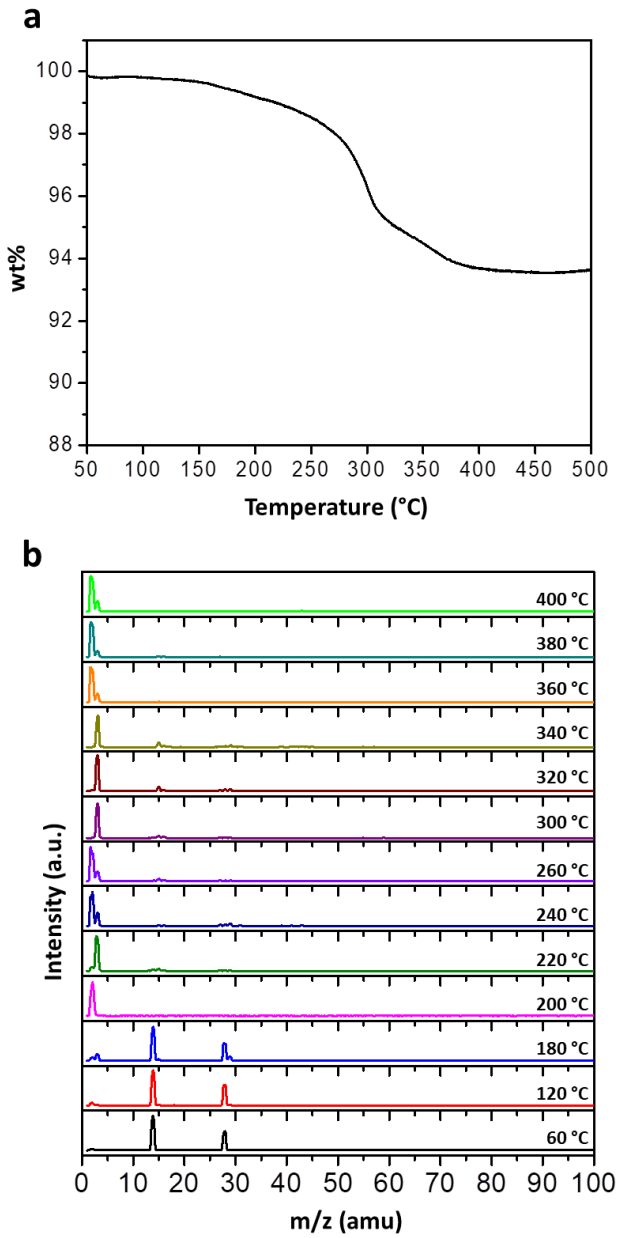

Figure S16. a) Thermogravimetric Analysis of pure γ-MBH, measured under Ar atmosphere with a heating rate of 5 K/min at ambient pressures. b) Mass spectra of γ-MBH without rGO at different temperatures in a range from 0-100 amu. Signals at m/z = 2 and 3 represent the release of H_2. Signals at m/z = 14 and 28 amu (spectra at 60°C, 120 °C and 180 °C) represent residual N_2 present in the reactor from the sample loading process inside a N_2 glovebox. At higher temperatures, minor signals at 15 amu represent BH_4 and around 26-28 amu represent B_2H_6.

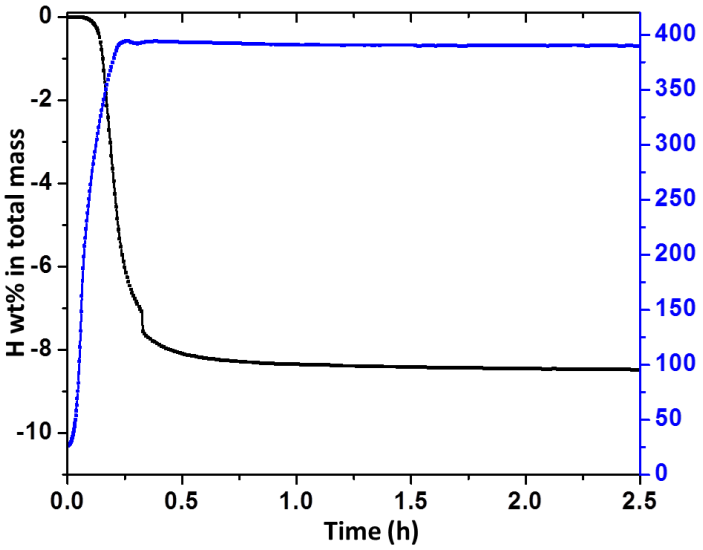

Figure S17. Hydrogen desorption characterization of γ-MBH without rGO at 390 °C and 0 bar.

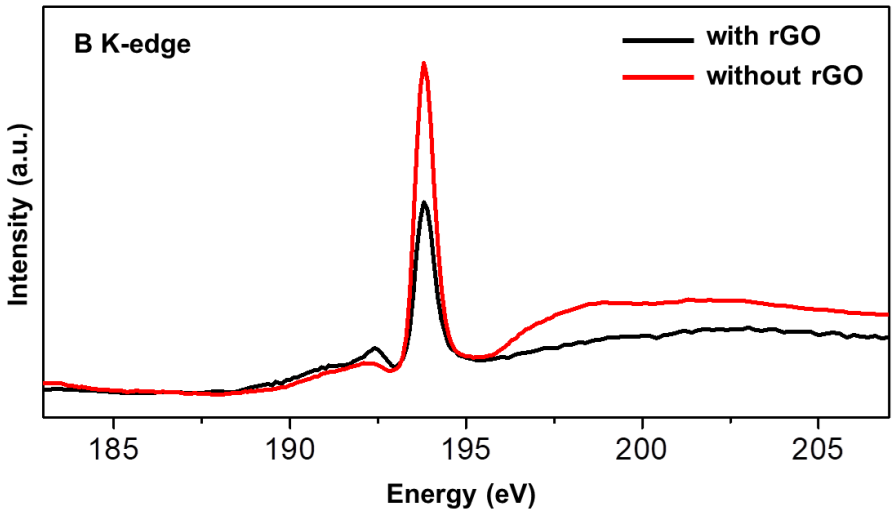

Figure S18. Boron K-edge XAS spectra of MBH with rGO (black) and without rGO (red).

REFERENCES

1. Filinchuk, Y.; Richter, B.; Jensen, T. R.; Dmitriev, V.; Chernyshov, D.; Hagemann, H. Porous and Dense Magnesium Borohydride Frameworks: Synthesis, Stability, and Reversible Absorption of Guest Species. *Angew. Chem., Int. Ed.* **2011**, *50*, 11162–11166.
2. Coelho, A. A. *TOPAS-Academic*, Version 4.1; Coelho Software: Brisbane, 2007.
3. Zavorotynska, O.; El-Kharbachi, A.; Deledda, S.; Hauback, B. C. Recent Progress in Magnesium Borohydride $Mg(BH_4)_2$: Fundamentals and Applications for Energy Storage. *Int. J. Hydrogen Energy* **2016**, *41*, 14387–14403.
4. Coelho, A. A. Indexing of Powder Diffraction Patterns by Iterative Use of Singular Value Decomposition. *J. Appl. Crystallogr.* **2003**, *36*, 86–95.
5. David, W.; Callear, S.; Jones, M.; Aeberhard, P.; Culligan, S.; Pohl, A.; Johnson, S.; Ryan, K.; Parker, J.; Edwards, P. P.; Nuttalld, C. J.; Amieiro-Fonseca A. The Structure, Thermal Properties and Phase Transformations of the Cubic Polymorph of Magnesium Tetrahydroborate. *Phys. Chem. Chem. Phys.* **2012**, *14*, 11800–11807.
6. Filinchuk, Y.; C, R.; Hagemann, H. Insight into $Mg(BH_4)_2$ with Synchrotron X-Ray Diffraction : Structure Revision, Crystal Chemistry, and Anomalous Thermal Expansion. *Chem. Mater.* **2009**, *21*, 925–933.